World Scientific
www.worldscientific.com

CHARACTERIZATION OF ZINC OXIDE NANOPOWDERS DOPED WITH MnO

M. EBRAHIMIZADEH ABRISHAMI, E. ATTARAN KAKHKI,
S. M. HOSSEINI[*,†], and A. KOMPANY

Department of Physics, Materials and Electroceramics Laboratory,
Ferdowsi University of Mashhad, Iran
[*]*seyedhosseini@um.ac.ir*
[†]*sma_hosseini@yahoo.com*

Pure ZnO and $Zn_{1-x}Mn_xO$ ($x = 0.02$ and 0.06) nanopowders have been synthesized by sol–gel technique at low temperatures. XRD results indicated that the crystal structure is hexagonal and there is no secondary phase. The compositional characterization of Mn-doped samples was investigated by EDX spectra. The size and morphology of nanoparticles were obtained by SEM and TEM images. Optical constants such as refractive index and extinction coefficient were evaluated from transmittance spectrum in UV region. The optical band gap energy showed a red-shift from 3.22 eV to 3.14 eV for pure and $Zn_{0.94}Mn_{0.06}O$, respectively. The Curie temperature of Mn-doped ZnO samples were determined and at room temperature no ferromagnetism state was observed.

Keywords: ZnO; Mn doping; sol–gel; nanopowder; optical properties.

PACS Number(s): 73.63.Bd, 74.25.Gz, 75.50.Pp

1. Introduction

Due to atom-like nanocrystalline size powders behaviors, new applications in optics, electronics, magnetics, and optoelectronics has been extended, effectively. In like manner, the variations in nano-zinc oxide properties are important, because ZnO has been extensively used in UV photodetectors,[1] thermoelectric and piezo-electric materials,[2,3] photodiodes, biosensors,[4] etc.[5] Furthermore, transition metal (TM)-doped ZnO has been attractive in a new application called spin-electronics (spintronics) applied in transparent transistors and etc.[6] Due to Dietl's[7] suggestion based on room temperature ferromagnetism (RTFM) in TM-doped ZnO, ZnO:Mn has recently engaged the researches.

The structural, magnetic, and optical properties are vigorously depended on synthesis technique. To remove the difficulties of solid-state reaction such as grain growth and achieve the uniform particle distribution and low temperature process,

---

[*]Corresponding author.

wet chemical preparations, such as sol–gel,[8] gel combustion,[9] and co-precipitation[10] have been widely applied.

ZnO is a direct wide band gap semiconductor crystallizes in wurtzite (hexagonal) structure with lattice parameters, $a = 3.2501$ Å and $c = 5.2071$ Å.[11] Reports on different growth orientation imply the sensibility of structural properties to synthesis method. Dispersion parameters such as refractive index, optical band gap energy, dispersion energy, etc. are experimentally determined and analyzed by theoretical models such as single effective oscillator,[12] Cauchy and Sellmeier equations.[13] Dispersion energy and long wavelength refractive index, obtained for bulk ZnO, is 17.1 eV and 1.91, respectively.[14]

In recent years, studies on bulk, thin films and nanocrystalline ZnO:Mn has reported different results in existence[15−17] or absence of RTFM.[18,19] In addition, some researches on ferromagnetism at low temperatures have been published with different Curie temperatures.[20,21]

In this paper, we have synthesized ZnO and $Zn_{1−x}Mn_xO$ ($x = 0.02$ and 0.06) nanopowders via sol–gel technique. Effect of Mn doping in lattice parameters and secondary phase were investigated. Dispersion parameters such as refractive index, extinction coefficient, dispersion energy, and optical band gap energy were determined by applying the transmittance and absorbance spectra in UV region. Magnetic Curie temperature was estimated by using Cedillo *et al.*[22] apparatus from measuring the magnetic permeability.

2. Experimental Procedures

$Zn_{1−x}Mn_xO$ ($x = 0.00, 0.02, 0.06$) were synthesized by sol–gel method at low temperatures. Zinc acetate dehydrate $Zn(CH_3COO)_2 \cdot 2H_2O$, manganese acetate tetrahydrate $Mn(CH_3COO)_2 \cdot 4H_2O$, acetic acid, and diethanolamine (DEA) were used as starting materials. Zinc acetate dehydrates and manganese acetate tetrahydrate are separately dissolved in mixture of isopropanol and distilled water. Clear solutions with appropriate amount of doping level were mixed together and stirred for 30 min heating at 40°C. The mixed acetic acid and DEA solution were added to material solution and stirred for 10 min. The molar ratios of acid acetic and DEA to cations were 2 and 1, respectively. A homogeneous and stable sol was obtained by refluxing the solution for 4 h at 110°C. Afterwards, the sol were placed in an 80°C heat bath to evaporate the solvents and achieve a generally approved gel. Then, the gel drying process was completed at temperatures of 140–150°C. The prepared powders were calcinated at 300 and 400°C for 2 h in air.

Phase identification and lattice constants values of nanopowders were analyzed by X-ray diffraction using Cu-K$_\alpha$ radiation ($\lambda = 1.54056$ Å). We used the energy dispersive X-ray (EDX) spectrophotometer to analyze the compositional properties. The size and morphology of nanoparticles are investigated by SEM and TEM images. The UV-Vis spectra were recorded from nanopowders ultrasonically dispersed in distilled water (0.01 g in 15 cc).[23,24]
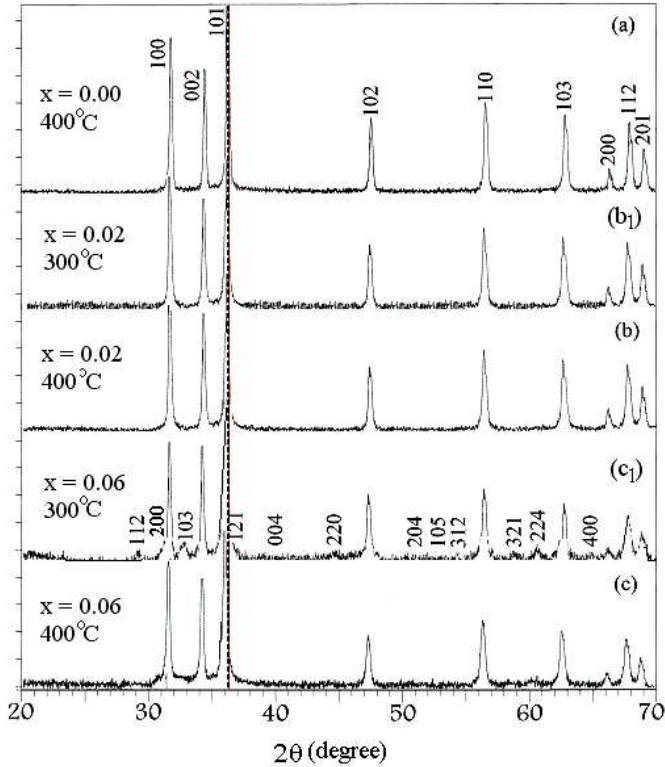
Fig. 1. XRD patterns for $Zn_{1-x}Mn_xO$: (a) $x = 0.00$, (b) $x = 0.02$ and (c) $x = 0.06$ calcinated at $400°C$, (b$_1$) $x = 0.02$ and (c$_1$) $x = 0.06$ calcinated at $300°C$. The guideline presents the shift as Mn concentration increases.

The Mn-doped samples grounded, pressed under 40 bars and sintered at $950°C$ for 4 h in order to measure the magnetic permeability versus temperature and hence determine the Curie temperature.

3. Results and Discussion

3.1. *Structural*

XRD patterns of pure ZnO and $Zn_{1-x}Mn_xO$ ($x = 0.02$ and 0.06) calcinated at $300°C$ and $400°C$ are shown in Fig. 1. The XRD analysis of ZnO nanopowder confirmed the presence of wurtzite in which the diffraction peaks are indexed in Fig. 1(a). Sharpness of peaks' intensity denotes the well crystalline nature of nanoparticles, which had occurred at low calcinated temperatures. The XRD pattern indicated a secondary phase in $Zn_{0.94}Mn_{0.06}O$ sample calcinated at $300°C$ (Fig. 1(c$_1$)). This phase belongs to $ZnMn_2O_4$ crystallizes in tetragonal structure, which was disappeared with increasing the calcinated temperature up to $400°C$.[25] The percent of the secondary phase has been approximately determined from the ratio of the impurity peaks intensity to the total peaks intensity. The portion
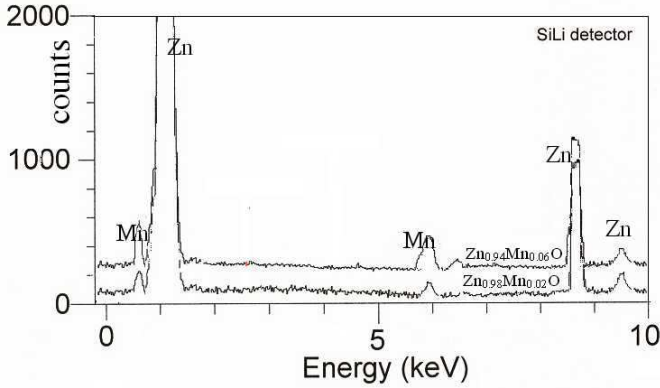
Fig. 2.   EDX spectra of $Zn_{0.98}Mn_{0.02}O$ and $Zn_{0.94}Mn_{0.06}O$ calcinated at $400°C$.

Table 1.   Variations in [101] peak positions and lattice parameters, a and c due to Mn doping and calcinated temperature.

Mn concentration (x)	Calcinations temperature (°C)	Structure	Position of peak [101] (°)	FWHM [101] (°)	Lattice parameter a (Å)	Lattice parameter c (Å)
(b$_1$) 0.02	300	Wurtzite	36.312	0.271	3.2470	5.1988
(c$_1$) 0.06	300	Wurtzite + Tetragonal	36.292	0.299	3.2478	5.2004
(a) 0.00	400	Wurtzite	36.317	0.248	3.2466	5.1981
(b) 0.02	400	Wurtzite	36.310	0.266	3.2472	5.1991
(c) 0.06	400	Wurtzite	36.285	0.282	3.2480	5.2014

of tetragonal phase from crystallization was estimated about 9%. The X-ray reflectance peaks of $ZnMn_2O_4$ structure are indexed in Fig. 1(c$_1$).

The precise composition of 0.02 and 0.06 Mn-doped samples nanoparticles was determined by an energy-dispersive analysis of X-rays (EDX) as shown in Fig. 2. The EDX spectra showed that the amount of Mn element increased depending on the concentrating of Mn in the solution.

The lattice parameters of hexagonal structure increased with growth of Mn concentration (Table 1). In spite of the fact that the ionic radius of isolated Mn^{+2} is 0.44 Å and much smaller than radius of isolated Zn^{+2} (0.74 Å), the ionic radius of Mn^{+2} in ZnO structure is 0.66 Å. This value is larger than radius of Zn^{+2} in structures and estimated to be about 0.60 Å therefore increasing the lattice constants as the doping level increase. Substitutions of Mn effectively shift the peaks positions to lower angles as indicated in Table 1 for [101] peak positions and the guideline in Fig. 1 presents this shift. This relation between lattice constants and peaks shift has also been noted by Karamat *et al.*[26] As Mn has another oxidation states like Mn^{+3} and Mn^{+4} therefore increasing lattice constants of wurtzite structure confirms only the substitution of Zn^{+2} with Mn^{+2} and not with other ionic states otherwise the
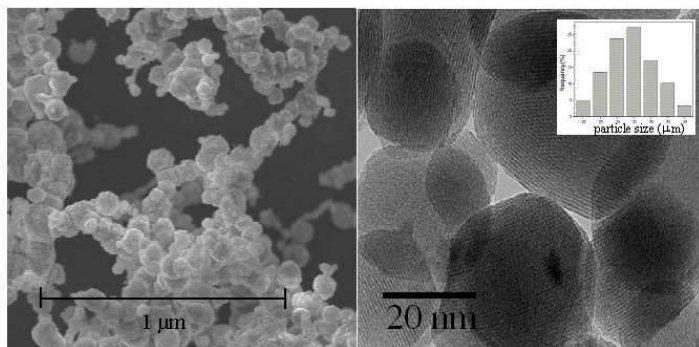
Fig. 3. (a) SEM, (b) TEM images of $Zn_{0.98}Mn_{0.02}O$ nanopowders calcinated at $400°C$. The inset of Fig. 3(b) is the histogram of the particle size distribution calcinated at $400°C$.

lattice constants must decrease.[27] Thus, full width at half maximum (FWHM) of [101] peak decreases as Mn concentration increases and this can be verified from crystalline size using the Scherrer's formula. The crystalline size using this formula was calculated to be 39.8 for pure and 37 and 35 nm for $x = 0.02$ and $x = 0.06$ Mn-doped ZnO calcinated at $400°C$, respectively.

The typical TEM images of the $Zn_{0.98}Mn_{0.02}O$ powders and the histogram of the particle size distribution calcinated at $400°C$ temperatures is presented in Fig. 3(b). From TEM analysis, the primary particle size of the powders can be evaluated. The maximum distribution of particle size of the $Zn_{0.98}Mn_{0.02}O$ nanopowder is approximately 35 nm in diameter. This value is in good agreement with the particles size calcinated from the Scherrer's formula.

3.2. *Optical properties*

The UV absorbance spectra of pure and Mn-doped ZnO nanopowders are shown in the insets of Fig. 4. Since the particles dispersed in water are nanosized and have much lower size than incident light wavelength, the absorbance spectra are acceptably reliable to determine the optical band gap energy, E_g. A reasonable method for investigating band gap energy E_g is finding the maxima in first derivative of absorbance with respect to photon energy spectra as marked with guidelines in Fig. 4.[23]

The optical band gap energy, E_g, of pure ZnO and $Zn_{1-x}Mn_xO$ ($x = 0.02$ and 0.06) nanopowders are shown in Fig. 4. The optical band gap energy decreases from 3.22 eV for pure ZnO to 3.17 eV and 3.14 eV for $Zn_{0.98}Mn_{0.02}O$ and $Zn_{0.94}Mn_{0.06}O$ dispersed powders respectively.

This red-shift in band gap energy was also reported in thin film[28] and bulk[29] ZnO:Mn. As the lattice parameter increases with growing Mn concentration, then we may expect to decreases the optical band gap. This phenomenon has also been discussed by Olguin *et al.*[30]
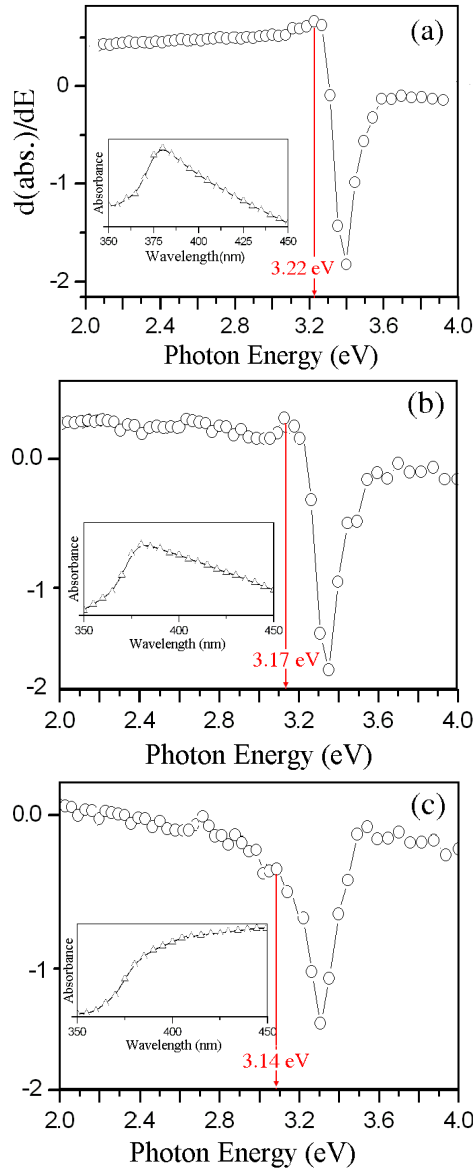
Fig. 4.   First derivative absorption spectra of (a) ZnO, (b) $Zn_{0.98}Mn_{0.02}O$ and (c) $Zn_{0.94}Mn_{0.06}O$, calcinated at $400°C$. Optical absorbance spectra of $Zn_{1-x}Mn_xO$ calcinated at $400°C$ are shown in the insets. The optical band gap energies are marked with guidelines.

The assistance of secondary phase on $Zn_{0.94}Mn_{0.06}O$ sample calcinated at $300°C$ can be revealed from the optical band gap energy as shown in the inset of Fig. 5. We can see after an absorbance peak at 377 nm, the spectrum increased following by a minima at 362 nm.
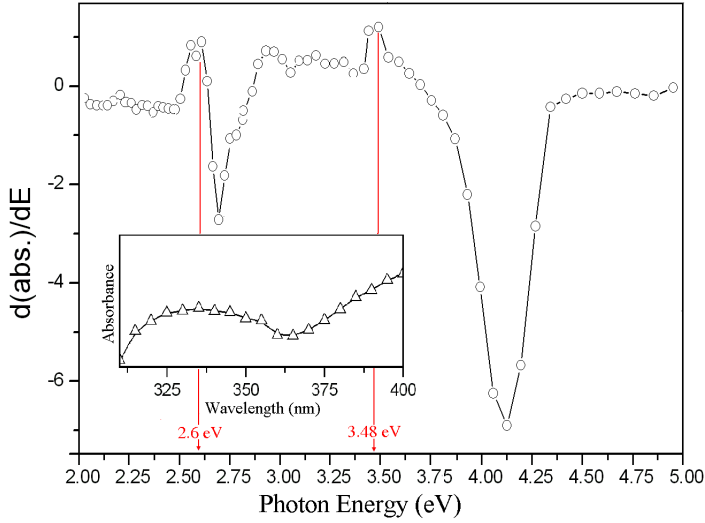
Fig. 5.   First derivative absorption spectra of $Zn_{0.94}Mn_{0.06}O$ calcinated at $300°C$. The inset shows the absorbance spectra.

This phenomenon does not occur in the absorbance spectra shown in Fig. 4 for mono-phase nanopowders. The first derivative spectra of $Zn_{0.94}Mn_{0.06}O$ calcinated at $300°C$, shown in Fig. 5, reveal two optical band gap energies that appear in 2.6 eV and 3.48 eV due to presence of two phases (tetragonal and wurtzite) in $Zn_{0.94}Mn_{0.06}O$ structure.

To obtain the refractive index of nanopowders, the Manifacier *et al.*[31] approach to Uv-Vis transmition spectrum was applied. The refractive index, $n(\lambda)$, and extinction coefficient, $k(\lambda)$, curves are shown in Fig. 6.

The refractive index decreases with increasing wavelength and extinction coefficient acts vice versa. The interactions between incident photons and electrons dominate on these variations. The best fits for refractive index curves using the three term Cauchy equation[13]:

$$n(\lambda) = A + \frac{B}{\lambda^2} + \frac{C}{\lambda^4}. \tag{1}$$

This equation helped us compare A, B and C parameters for pure and Mn-doped ZnO. The obtained values are summarized in Table 2. In addition, refractive index data below the interband absorption edge can be analyzed according to a single effective oscillator model of Wemple–DiDomenico.[14]

$$n^2(E) = 1 + \frac{E_d E_0}{E_0^2 - E^2}, \tag{2}$$

where E, E_0 and E_d are the photon energy, effective dispersion oscillator energy, and dispersion energy, respectively. The average strength of interband optical transitions is clarified by dispersion energy, E_d. Both of E_0 and E_d were obtained by plotting
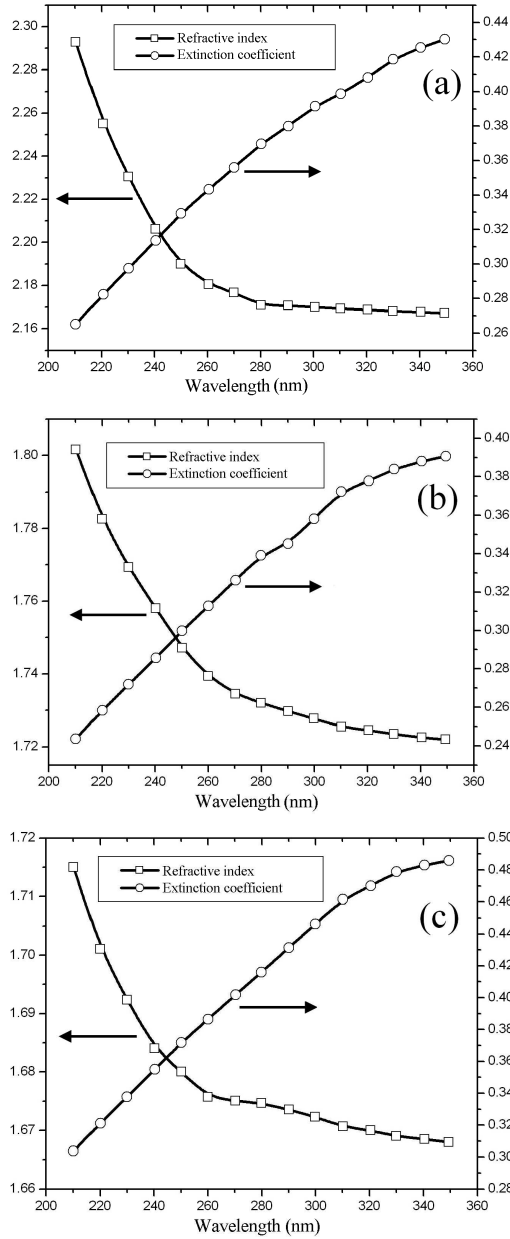
Fig. 6. Refractive index and extinction coefficient of $Zn_{1-x}Mn_xO$ nanopowders calcinated at $400°C$, (a) $x = 0.00$, (b) $x = 0.02$ and (c) $x = 0.06$.

$(n^2 - 1)^{-1}$ versus E^2 and determining the slope and intercept of line to vertical axis (Fig. 7). The calculated values for nano-ZnO and $Zn_{1-x}Mn_xO$ ($x = 0.02$ and 0.06) are listed in Table 2. The parameter E_d for ZnO wurtzite crystal structure
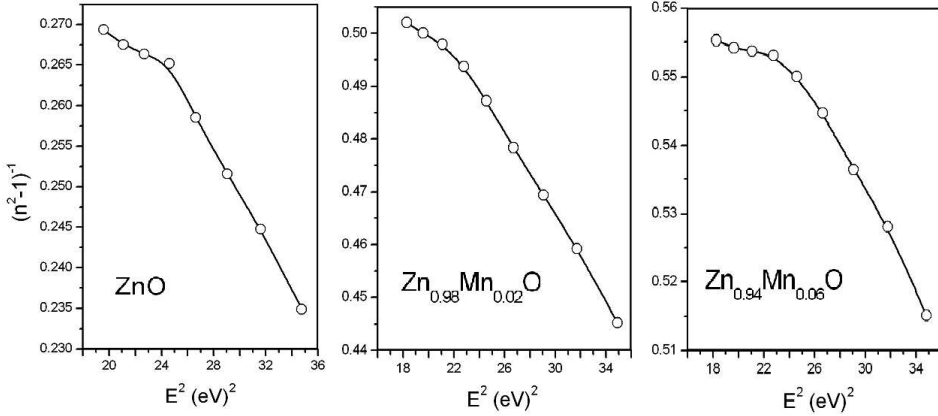
Fig. 7. The plots $(n^2 - 1)^{-1}$ versus E^2 for undoped and Mn-doped samples which are applied to calculate dispersion and effective dispersion oscillator energy.

Table 2. Dispersion parameters of $Zn_{1-x}Mn_xO$ nanopowders calcinated at $400°C$.

Mn concentration			Cauchy equation		Sellmeier equation	Single effective oscillator model	
(x)	E_g (eV)	A	B (μm^2)	C (μm^4)	n_∞	E_0 (eV)	E_d (eV)
0.00	3.22	2.83	-0.93×10^{-4}	6.42×10^{-3}	1.97	6.85	21.30
0.02	3.17	2.33	-1.20×10^{-4}	4.97×10^{-3}	1.68	6.65	14.21
0.06	3.14	2.35	-1.61×10^{-4}	5.34×10^{-3}	1.63	6.59	12.99
0.00	3.34[a]	1.94	-1.97×10^{-4}	7.09×10^{-3b}	1.91[c]	6.50	17.10[c]

[a]Band gap energy of bulk ZnO.[13]
[b]Cauchy parameters for bulk ZnO.[13]
[c]Bulk ZnO.[14]

is 21.3 and it is clearly observed that dispersion energy, E_d, sensibly decreases with progressive growth in Mn concentration. This can be easily understood by taking account of interband transitions in magnetic atoms.[12] In this manner, the Eq. (2) must be substituted by two oscillator description of refractive index. The parameters E_0 for all samples approximately satisfies the relationship of $E_0 \approx 2E_g$ supposed by Wemple *et al.*[14] Furthermore, the long wavelength refractive index can be studied by using the Sellmeier equation[13]:

$$\frac{n_\infty^2 - 1}{n^2 - 1} = 1 - \left(\frac{\lambda_0}{\lambda}\right)^2, \tag{3}$$

where n_∞ and λ_0 are long wavelength refractive index and oscillator wavelength, respectively. Mn doping caused a sudden decrease in long wavelength refractive index, but increasing the doping up to $x = 0.06$, absolutely did not effect so much on n_∞ in comparison with $x = 0.02$ doping (Table 2).
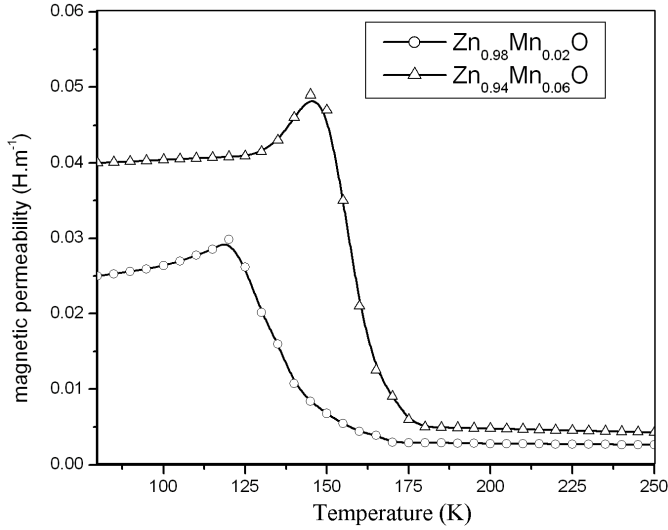
Fig. 8.   The magnetic permeability versus temperature for $Zn_{0.94}Mn_{0.06}O$ and $Zn_{0.98}Mn_{0.02}O$ powders calcinated at 400°C.

3.3.   *Magnetic properties*

Plotting magnetic permeability of Mn-doped samples versus temperature helped to determine the Curie temperature and tested the homogeneity of samples.[32] Permeability is obtained by measuring the inductance of the sample in a coil on an impedance bridge at different temperatures. Sudden falling down the permeability in the plot shows the Curie point. We used the apparatus was suggested by Cedillo *et al.*[22] for ferromagnetic oxides.

The 400°C-calcinated Mn-doped samples in a coil were placed in a heat inertia chamber. Samples were cooled by liquid nitrogen and warmed up gradually with a constant rate. The inductance was measured by LCR meter (Topward 5020) at 1 KHz.

The variation of magnetic permeability versus temperature is shown in Fig. 6. The Curie point is determined by drop point of the plot which lies in the range 150–170 K for $Zn_{0.94}Mn_{0.06}O$ and 135–150 K for $Zn_{0.98}Mn_{0.02}O$. The large value of verticality slope at Curie point in Fig. 8 approved the chemical homogeneity of samples.

4.   Conclusions

Single phase pure and Mn-doped ZnO nanopowders have been synthesized by sol–gel technique calcinated at 400°C with crystalline size about 30–40 nm. Optical band gap energy decreased as Mn concentration growth. Static refractive index showed a decreasing from 1.97 to 1.63 for pure ZnO and $Zn_{0.94}Mn_{0.06}O$, respectively. Single effective oscillator model clarified the Mn-doping effects on optical transition

bands. Although the ferromagnetic behavior was observed in Mn-doped samples, the Curie temperature was estimated between 135 and 150 K for $Zn_{0.98}Mn_{0.02}O$ and 150–170 K for $Zn_{0.94}Mn_{0.06}O$.

References

1. O. Lupan, L. Chow, G. Chai, L. Chernyak, O. L. Tirpak and H. Heinrich, *Phys. Stat. Sol.* **205** (2008) 2673–2678.
2. Y. Tanaka, T. Ifuku, K. Tsuchida and A. Kato, *J. Mater. Sci. Lett.* **16** (1997) 155–157.
3. P. X. Gao and Z. L. Wang, *J. Appl. Phys.* **97** (2005) 0443041-7.
4. S. A. Kumar and S. M. Chen, *Appl. Anal. Lett.* **41** (2008) 141–158.
5. D. C. Look, *Mater. Sci. Engin. B* **80** (2001) 383–387.
6. S. J. Pearton, D. P. Norton, Y. W. Heo, L. C. Tien, M. P. Ivill, Y. Li, B. S. Kang, F. Ren, J. Kelly and A. F. Hebard, *J. Elect. Mater.* **35** (2006) 862–868.
7. T. Dietl, H. Ohno, F. Matsukura, J. Cibert and D. Ferrand, *Science* **287** (2000) 1019–1022.
8. V. K. Sharma, R. Xalxo and G. D. Varma, *Cryst. Res. Technol.* **42** (2007) 34–38.
9. J. Luo, J. K. Liang, Q. L. Liu, Y. Zhang, B. J. Sun and G. H. Rao, *J. Appl. Phys.* **97** (2005) 086106-086106-3.
10. O. D. Jayakumar, H. G. Salunke, R. M. Kadam, M. Mohapatra, G. Yaswant and S. K. Kulshreshta, *Nanotechnology* **17** (2006) 1278–1285.
11. E. H. Kisi and M. M. Elcombe, *Acta. Cryst.* **45** (1989) 1867–1870.
12. S. H. Wemple, *Phys. Rev. B* **7** (1973) 3767–3777.
13. Ü. Özgür, Y. I. Alivov, C. Liu, A. Teke, M. A. Reshchikov, S. Doğan, V. Avrutin, S. J. Cho and H. Morkoç, *J. Appl. Phys.* **98** (2005) 041301.
14. S. H. Wemple and M. DiDidomenico, *Phys. Rev. B* **3** (1971) 1338–1352.
15. N. A. Theodoropoulou, A. F. Hebard, D. P. Norton, J. D. Budai, L. A. Boatner, J. S. Lee, Z. G. Khim, Y. D. Park, M. E. Overberg, S. J. Pearton and R. G. Wilson, *Solid State Electron.* **47** (2003) 2231–2235.
16. Y. W. Heo, M. P. Ivill, D. P. Norton, S. J. Peartona, J. G. Kelly, R. Rairigh, A. F. Hebard and T. Steiner, *Appl. Phys. Lett.* **84** (2004) 2292–2294.
17. M. Diaconua, H. Schmidta, H. Hochmutha, M. Lorenza, G. Benndorfa, J. Lenznera, D. Spemanna, A. Setzera, K. W. Nielsenb, P. Esquinazia and M. Grundmanna, *Thin Solid Films* **486** (2005) 117–121.
18. S. Kolesnik and B. Dabrowski, *J. Appl. Phys.* **96** (2004) 5379–5381.
19. G. Lawes, A. S. Risbud, A. P. Ramirez and R. Seshadri, *Phys. Rev. B* **71** (2005).
20. S. Lee, H. S. Lee, D. S. Kim, D. Y. Kim and Y. D. Woo, *J. Korean Phys. Soc.* **45** (2004) 1304–1307.
21. V. A. L. Roy, A. B. Djurišić, H. Liu, X. X. Zhang, Y. H. Leung, M. H. Xie and J. Gao, *Appl. Phys. Lett.* **84** (2004) 756–758.
22. E. Cedillo, J. Ocampo, V. Rivera and R. Valenzuela, *J. Phys. E: Sci. Instrum.* **13** (1980) 383–386.
23. A. E. Morales, E. S. Mora and U. Pal, *Revista Mexicana de Físicas* **53** (2007) 18–22.
24. M. Bangal, S. Ashtaputre, S. Marathe, A. Ethiraj, N. Hebalkar, S. W. Gosavi, J. Urban and S. K. Kulkarni, *Hyperfine Interact.* **160** (2005) 81–94.
25. D. Milivojević, J. Blanuša, V. Spasojević, V. Kusigerski and B. B. Stojić, *Solid State Commun.* **141** (2007) 641–644.
26. S. Karamat, S. Mahmood, J. J. Lin, Z. Y. Pan, P. Lee, T. L. Tan, S. V. Springham, R. V. Ramanujan and R. S. Rawat, *Appl. Surf. Sci.* **254** (2008) 7285–7289.

27. M. E. Abrishami, S. M. Hosseini, E. A. Kakhki, A. Kompany and M. Ghasemifard, *Int. J. Nanosci.* (2009) accepted.
28. S. Maensiri, C. Masingboon, V. Promarak and S. Seraphin, *Opt. Mater.* **29** (2007) 1700–1705.
29. R. A. Smith, *Semiconductors*, 2nd edn. (Cambridge University Press, Cambridge, 1978).
30. D. Olguin, R. Baquero and R. de Coss, *Revista Mexicana de Físicas* **47** (2001) 43–49.
31. J. C. Manifacier, J. Gasiot and J. P. Fillard, *J. Phys. E: Sci. Instrum.* **9** (1976) 1002–1004.
32. A. Globus, P. Duplex and M. Guyot, *IEEE Trans. Magn.* **MAG-7** (1971) 617–622.